Progress In Electromagnetics Research C, Vol. 75, 63–73, 2017

Compact 2×1 MIMO Antenna System for LTE Band

A. Christina Josephine Malathi* and D. Thiripurasundari

Abstract—A compact 2×1 multiple input multiple output (MIMO) antenna system is designed to operate in the LTE band 40 (2.3–2.4) GHz. The proposed antenna consists of two circular patches fed using microstrip line. The antenna was initially designed to resonate at 5 GHz. Size reduction of 55.17% compared to conventional patch antenna is obtained after the inclusion of circular complementary split ring resonator (CSRR) in the ground plane. The resonating frequency was shifted to 2.34 GHz, thereby the board size is compact ($50 \times 25 \times 1.6\,\text{mm}^3$). The designed antenna covers a bandwidth of 2.3 to 2.374 GHz with a maximum return loss of -27 dB at 2.34 GHz and isolation of -33.5 dB between the ports. The simulated correlation coefficient is approximately zero, and the total active reflection coefficient is 0.142 at the resonating frequency which are within the acceptable limits. The realized gain for the antenna is -8.9 dB.

1. INTRODUCTION

Long Term Evolution (LTE) is the fourth generation wireless communication networks based on internet protocol (IP). It provides higher throughput, wider bandwidth and improved handoff capabilities compared to third generation networks. It also offers theoretical data rates of 300 Mbps and 75 Mbps for the downlink and uplink channels, respectively [1, 2]. LTE uses MIMO technology to improve the efficiency of using radio spectrum. MIMO antenna is expected to be a key element to support LTE systems. MIMO depends on the use of multiple antennas on the transmitting and receiving sides thereby increasing the channel capacity without the need of additional bandwidth or power. There is an increasing demand for making new MIMO antenna systems that are compact and compatible with user terminals and other wireless portable devices. The integration of multiple antennas on the user mobile terminals is a design challenge that has been given considerable attention by researchers, due to the inherent size and inter-antenna coupling limitations. Hence it is important to make antennas that have enhanced channel capacity, bandwidth, gain, and diversity performance. These requirements make the design of MIMO antenna systems challenging. There are a number of techniques available in the literature for isolation [3] and antenna miniaturization. Material loading is to use a substrate with high relative permittivity or loading high permittivity bar on a low permittivity substrate. As the length and width of the patch are inversely proportional to the square root of ε_r, use of high permittivity substrate results in miniaturization at the cost of reduced efficiency and lower bandwidth due to increased surface wave excitation within the substrate [4]. Loading of high dielectric substrate requires expensive material. Miniaturization up to four times can be achieved by reshaping the antenna by using fractal antenna or by cutting slots on the patch. This method suffers from high ohmic losses leading to low radiation efficiency with complex geometry and poor polarization purity [5, 6]. Miniaturization up to four times can be achieved by folding the antenna and by using shorting posts. This technique suffers from decreased directivity and gain in addition to complex antenna geometry [7, 8]. By introducing slots, the current path within the patch area is increased lowering the resonant frequency leading to 40–75% of

Received 22 February 2017, Accepted 31 May 2017, Scheduled 15 June 2017
* Corresponding author: Andrews Christina Josephine Malathi (achristina@vit.ac.in).
The authors are with the VIT University, Vellore, India.

side reduction. It provides wide bandwidth, but affects the radiation characteristics and provides poor polarization purity [9]. By introducing defects or slots in the ground plane, size reduction up to eight times is achieved but with lower efficiency, increased back lobe level and narrow bandwidth [10, 11]. Metamaterials such as ENG, MNG or DNG inspired antennas provide high degree of miniaturization with limited bandwidth, low efficiency and complex geometry [12–17].

Various isolation techniques available such as antenna placement, orientation, decoupling network, defected ground structure, neutralization line, parasitic element and metamaterial have been reported for mutual coupling reduction. The electromagnetic interaction between the antenna elements in an antenna array is called mutual coupling. The mutual coupling reduces the antenna efficiency and alters the radiation pattern and its performance. Antenna placement also plays a significant role in isolation enhancement. Placing antennas adjacently at distances less than $\lambda/4$ causes high coupling. The standard board size is taken quarter wavelength from all sides of the patch. The ground coupling and field coupling can be minimized if the adjacent antennas are oriented in quadrature with each other (i.e., 90°). When two linearly polarized antennas are placed orthogonally to each other, they can decrease the mutual coupling and offer polarization diversity [18, 19]. The mutual coupling between adjacent antenna elements can be reduced by using decoupling networks such as 180° hybrid coupler and coupled resonator [20, 21]. These networks will decouple the input ports of adjacent antennas by providing an electromagnetic field such that it cancels the EM fields introduced between the adjacent antennas. Indirect coupling is achieved by decoupling network composed of two directional couplers. These couplers are connected by two sections of transmission line of length 0.635λ. By connecting the two couplers, an indirect coupling with sufficient magnitude and phase is provided, which is used to cancel out the direct coupling caused by space waves and surface waves between array elements. The measured mutual coupling was reduced to below -58 dB at the center frequency of 7.5 GHz.

Parasitic elements are used between the antennas to cancel part of the coupled fields between them by creating an opposite coupling field thus reducing the overall coupling on the victim antenna using parasitic tape and stepped impedance resonator as parasitic element [22, 23]. A T-shaped ground stub with a slot is used between the two square monopole elements to reduce mutual coupling in [24]. The T-shaped ground stub improves the matching of antenna, and the slot within it improves the isolation by reflecting radiation from the radiators. The mutual coupling between adjacent MIMO antenna elements can be reduced by introducing defects within the ground plane. The defects act as band reject filters and suppress the coupled fields between the adjacent antenna elements by decreasing the current on the ground plane and hence increasing the separation between the elements. The defects can be slitted ground and circular split ring [25, 26]. In [27], an H-shaped DGS $W_d \times L_d$ of dimension $2 \times 20\,\text{mm}^2$ with centre gap of 0.2 mm is etched under the square patch of dimension $52 \times 52\,\text{mm}^2$ functions as a band stop filter by suppressing the higher order harmonics greater than 20 dB at a resonant frequency of 1.82 GHz.

Isolation can be improved by using a neutralization line (NL). By selecting an appropriate length of the NL, the excitation phase current is inverted. This inverted current is fed to the nearby antenna to reduce the amount of coupled current. NL can be a line or annular ring between the elements [27, 28]. Two printed short circuited inverted-U shaped monopole-antennas of dimension 8 mm × 14.5 mm are placed on the opposite corners of the substrate with a spacing of 14 mm with a dimension of 13 mm × 14 mm for ground portion in between them [29]. That space can be utilized for placing the feeding network. The small ground portion of the system ground plane was removed only 1.5 mm inwards from the top edge to accommodate a thin, printed neutralization line that links to the monopoles relatively close to the antenna feed ports. With the inclusion of neutralization line, antenna port isolation is increased. The antenna port isolation less than -19 dB was obtained. Metamaterials (MTM) are used for isolation enhancement between adjacent elements due to the presence of a band gap in their frequency response. The two most widely used MTM structures for isolation improvement between neighboring elements are the use of split-ring resonators (SRR) and Complementary Split Ring Resonator (CSRR). CSRRs are the negative image of SRRs (Babinet's principle), and an axial time varying electric field is necessary to excite the rings that create an effective negative ε medium and inhibit signal propagation at resonance. In [30], two cross printed dipole antennas are perpendicularly placed on a ground plane and excited by two similar microstrip baluns. In order to further broaden the impedance bandwidth, the CSRRs are etched on the patch at symmetrical positions. CSRRs act

as a negative permittivity bandstop filter. CSRR can also be employed in array structures. Wahid et al. have proposed a novel array antenna structure where the array antenna is loaded with the minimum number of CSRRs. Side-lobe level reduction of around 4.3 dB is reported [31].

In this paper, a novel design of compact 2×1 (two-element) MIMO patch with two identical circular patch antennas with CSRRs in the ground plane is proposed. The operating band of the proposed antenna is the LTE band with a resonant frequency of the antenna elements centered at 2.34 GHz. The characteristic study of single unit cell CSRR is done using HFSS by obtaining the relative permittivity of CSRR. Also the effect of antenna with CSRR and the effect of CSRR position with antenna are analyzed. More than 50% reduction in the size of the individual patch is achieved through CSRR loading, thus allowing the accommodation of the two patch antennas in an area of $50 \times 25\,\text{mm}^2$ with 10 mm spacing between them. The total size of the proposed MIMO antenna system board is $50 \times 25 \times 1.6\,\text{mm}^3$. The paper is structured as follows. Section 2 discusses the design of complementary split ring resonator. Section 3 describes the design of antenna. Section 4 presents and associates the simulation and measured results, and Section 5 concludes the paper.

2. COMPLEMENTARY SPLIT RING RESONATOR

The CSRR is a resonant structure which behaves as an LC tank circuit [32]. It interacts with the axial electric field and exhibits negative permittivity near the resonant frequency. The geometry of the CSRR is shown in Fig. 1(a). The radius of the inner ring, outer ring of CSRR, width of each ring, spacing between the rings and the width of slit in the rings are denoted as R_1, R_2, w, g, and k, respectively. Its dimension is tabulated in Table 1.

Single unit cell CSRR was simulated using HFSS to understand the behavioural characteristics from the relative permittivity obtained. Nicolson Ross Weir demonstrated the extraction of relative permittivity using S parameters [33–35] and is given by,

$$V_1 = S_{11} + S_{21}, \tag{1}$$

Table 1. CSRR dimensions.

Description	Parameter	Dimensions
Inner radius of the CSRR ring	R_1	3.4938
Outer radius of the CSRR ring	R_2	4.1938
Width of the rings	w	0.5 mm
Spacing between the rings	g	0.5 mm
Width of the slit	k	0.2 mm

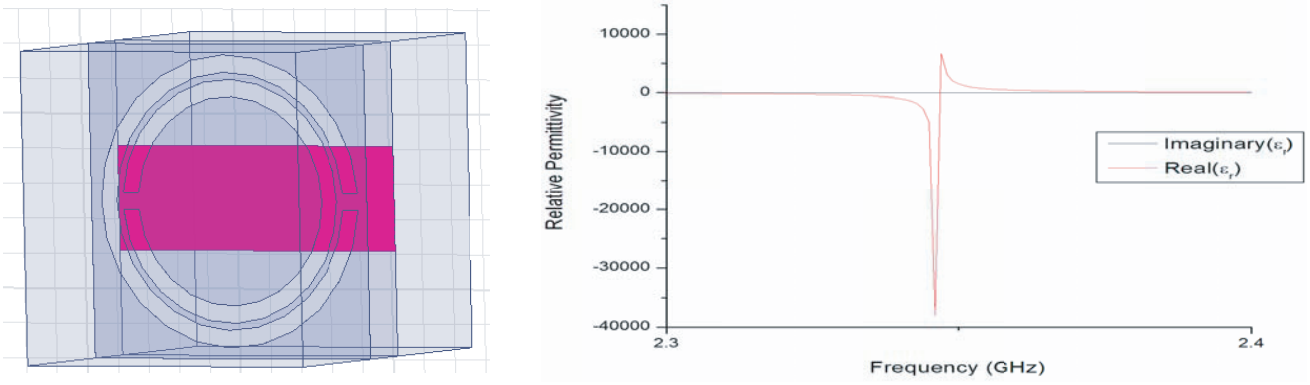

(a) (b)

Figure 1. (a) Unit cell CSRR. (b) Relative permittivity vs. frequency for a single unit cell CSRR

$$V_2 = S_{21} - S_{11} \tag{2}$$

$$\varepsilon_r = \frac{2c(1-V_1)}{\omega di(1+V_1)}, \tag{3}$$

$$\mu_r = \frac{2c(1-V_2)}{\omega di(1+V_2)} \tag{4}$$

where ω is the frequency in radian; c is the velocity of light in m/s; d is the thickness of the substrate; i corresponds to imaginary part; V_1 is the voltage maxima; V_2 is the voltage minima. From S parameters, relative permittivity was plotted using Equations (1), (2), (3) and (4). The negative value of relative permittivity was obtained at the desired resonant frequency of 2.34 GHz clearly exhibiting that CSRR acts as a bandstop filter shown in Fig. 1(b).

3. DESIGN OF THE ANTENNA

A circular patch antenna of dimension $25 \times 25\,\text{mm}^2$ was initially designed to resonate at 5 GHz using an FR4 substrate with a dielectric constant 4.4 and thickness 1.6 mm. The patch antenna was excited using 50 Ω microstrip line. The geometry of the antenna is shown in Fig. 2.

Initially the antenna was designed at a frequency (5 GHz) greater than the desired resonant frequency (2.34 GHz). To reduce the size of the antenna, a CSRR was etched out underneath the patch in the ground plane as shown in Fig. 2(b). Due to the anisotropic nature of the CSRR, its location below the patch affects the resonant frequency of the patch antenna [36]. The placement of the

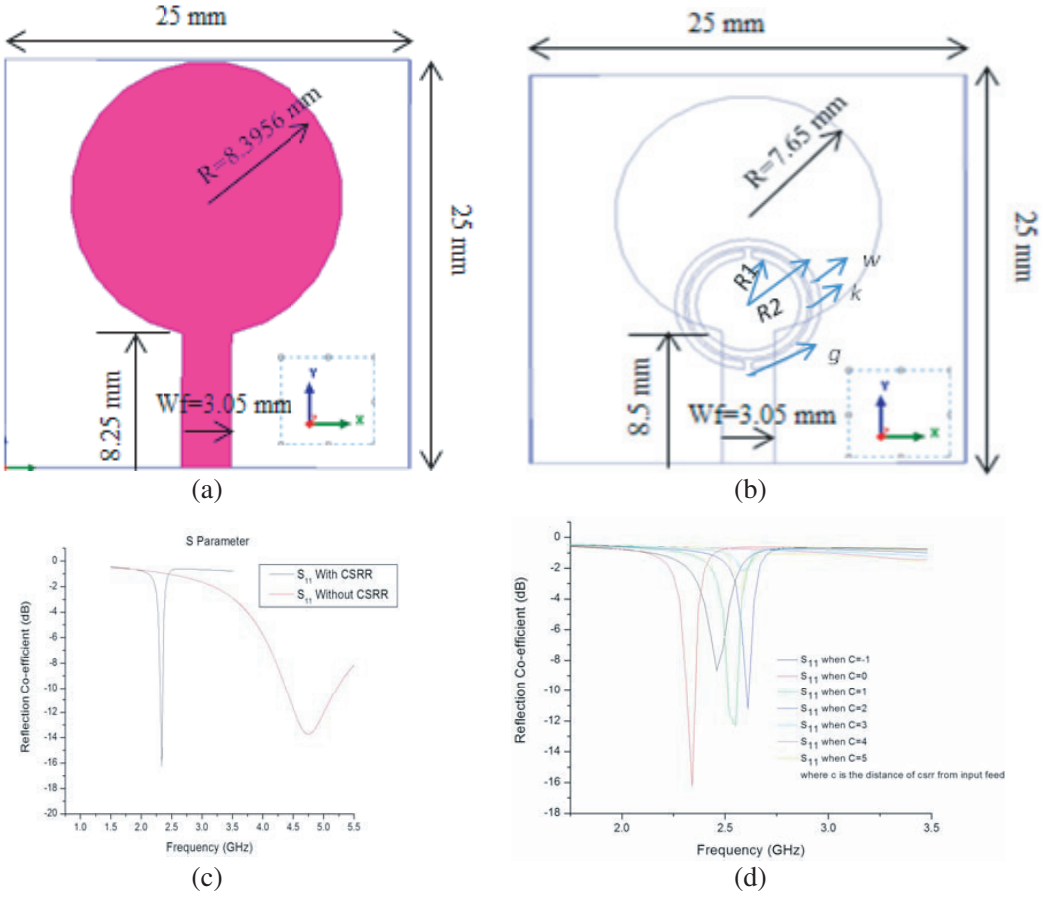

Figure 2. (a) Single patch antenna structure. (b) Single patch antenna with CSRR structure. (c) Comparison of return loss with and (d) CSRR position variation without CSRR for single patch antenna.

CSRR underneath the patch in the ground plane makes the patch act as bandpass filter at the resonant frequency. As noted in Fig. 2(d) when the CSRR is shifted away from the feed, the resonating frequency is increasing, and when it is near the feed, the resonant frequency is again increasing. Hence optimal

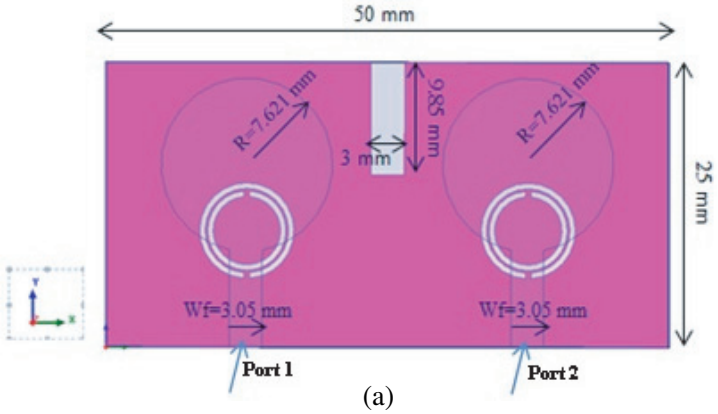

(a)

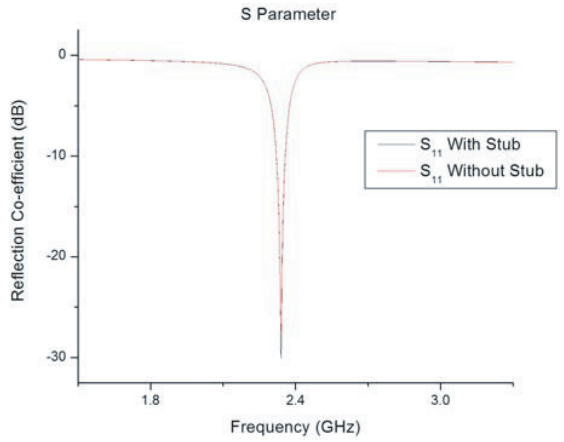

(b)

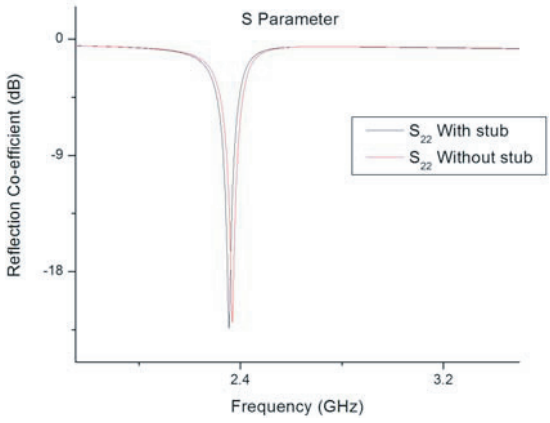

(c)

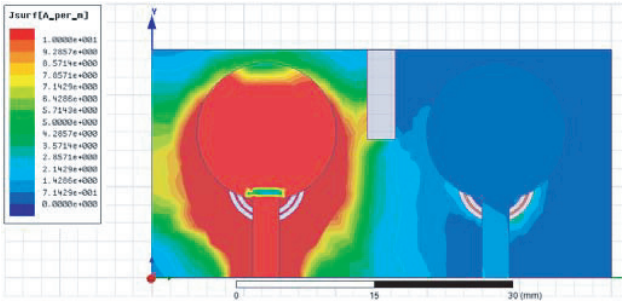

(d)

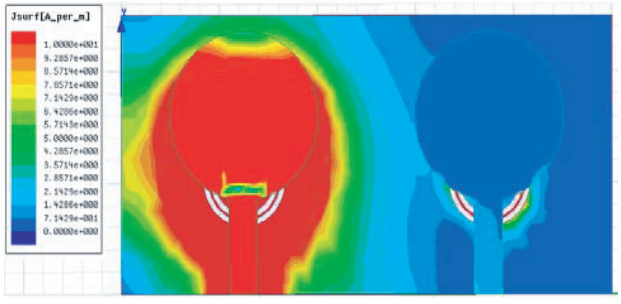

(e)

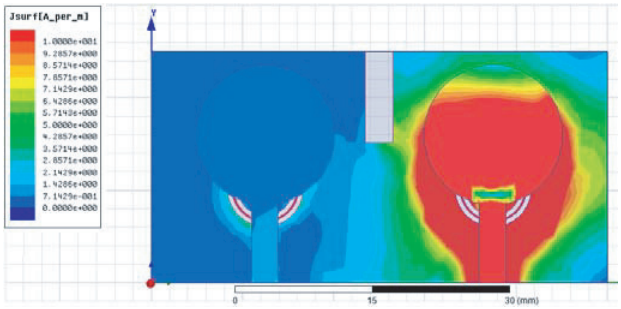

(f)

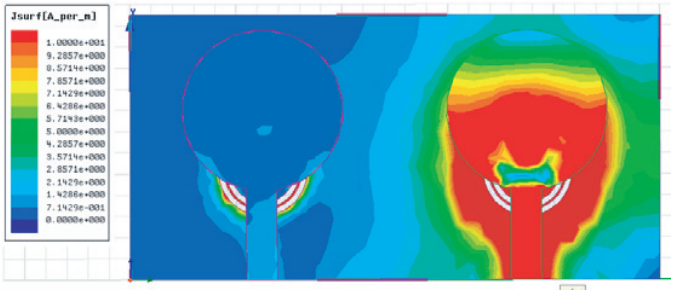

(g)

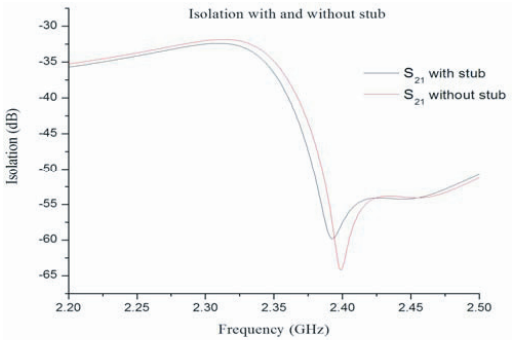

(h)

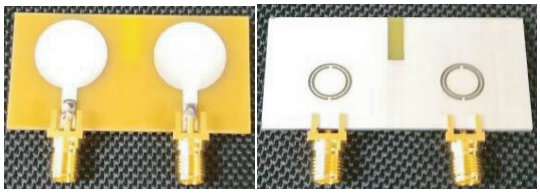

(i) (j)

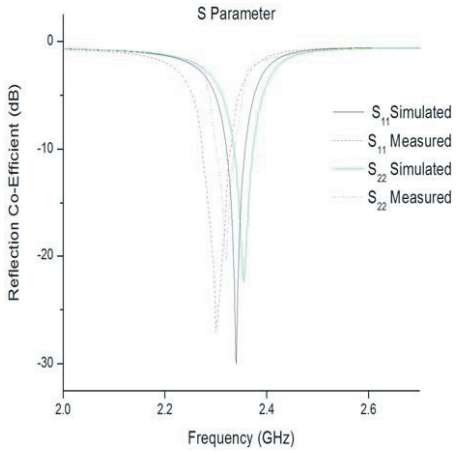

(k)

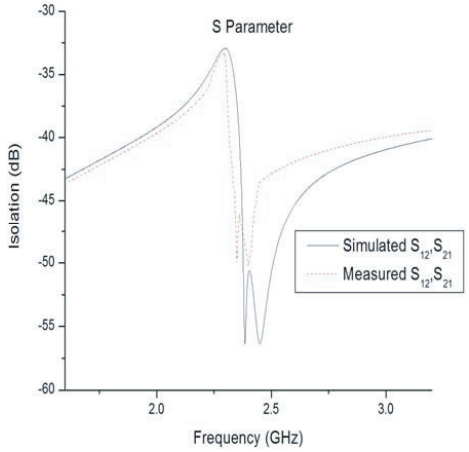

(l)

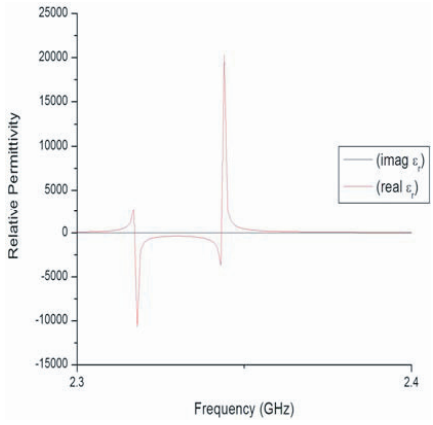

(m)

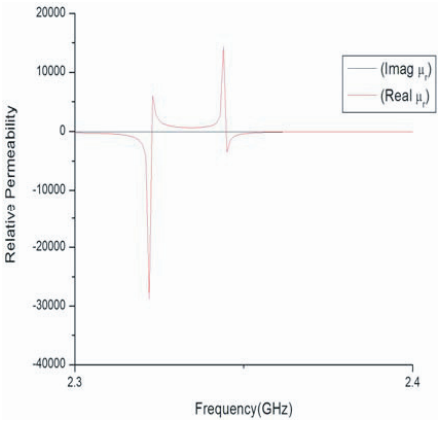

(n)

Figure 3. (a) 2×1 MIMO antenna structure with stub. Comparison of return loss for 2×1 MIMO patch antenna (b) with stub, (c) without stub. (d) Current distribution with stub when antenna 1 excited and element 2 terminated with $50\,\Omega$ load at 2.34 GHz. (e) Current distribution without stub when antenna 1 excited and element 2 terminated with $50\,\Omega$ load at 2.34 GHz. (f) Current distribution with stub when antenna 2 excited and element 1 terminated with $50\,\Omega$ load at 2.34 GHz. (g) Current distribution without stub when antenna 2 excited and element 1 terminated with $50\,\Omega$ load at 2.34 GHz. (h) Isolation with and without stub. Fabricated MIMO antenna system: (i) Front side (j) Back side. (k) Return Loss for 2×1 MIMO patch antenna. (l) Isolation for 2×1 MIMO patch antenna. (m) and (n) Relative permittivity and relative permeability vs. frequency for the antenna with CSRR.

position of CSRR is required for the antenna to resonate at 2.34 GHz using HFSS. The antenna with CSRR resonates at 2.34 GHz and without CSRR resonates at 4.8 GHz as shown in Fig. 2(c) covering a bandwidth of 2.3 to 2.374 GHz occupying the LTE band. Introducing CSRR for a single patch, there is a shift in the resonant frequency with a size reduction of 55%.

4. RESULTS AND DISCUSSION

The simulation was further extended for MIMO configuration by designing two circular patch antennas of dimension $50 \times 25 \times 1.6\,\text{mm}^3$ as shown in Fig. 3(a).

The simulation results for the return loss without stub were observed to be -27.35 dB at the resonant frequency of 2.34 GHz with an isolation of -33.3 dB covering a bandwidth of 2.3 to 2.373 GHz, and the comparative plots for both with and without stub are shown in Figs. 3(b) and (c).

It was observed that there was a shift in resonating frequency of the second patch, and hence a stub was inserted between two patches. The purpose of the stub between the two antenna elements is that it increases the electrical length between the two elements, thereby there is a shift in the resonant frequency of the second patch [37] in the lower side, i.e., (2.31 GHz). With the introduction of stub, the current distribution path is increased as a result of decrease in the resonance frequency. The effect of the stub is analyzed using current distribution plot which describes the field distribution from the radiating elements. When antenna 1 is excited with and without slot, the current distribution is maximum and same as shown in Figs. 3(d), 3(e). When antenna 2 is excited without slot, the current distribution is reduced, and with the introduction of slot, the current distribution is maximum and shown in Figs. 3(f), 3(g).

Also the isolation between the two elements is increased from -33 dB to -35 dB with the introduction of stub as shown in Fig. 3(h).

The front and back views of photographs of the fabricated antenna are shown in Figs. 3(i) and (j). The simulation result for the isolation with stub was observed to be -35.51 dB at the resonant frequency of 2.34 GHz, and the measured result for the isolation is -33.5 dB at the resonant frequency of 2.3 GHz, as shown in Figs. 3(k) and (l). The designed antenna covered a bandwidth of 2.3 to 2.372 GHz using simulation whereas 2.26 to 2.34 GHz for the measurement.

To study the effect of CSRR on MIMO antennas, permittivity and permeability are computed, and both are negative. The plot is done using Equations (1)–(4) and shown in Figs. 3(m) and (n) for the antenna structure, clearly explaining the concept of bandpass filter at the resonant frequency of 2.34 GHz. Negative values of permittivity and permeability are the characteristic for bandpass filter. A single unit cell CSRR acts as bandstop filter, and the inclusion of CSRR underneath the patch also acts as bandpass filter at resonant frequency.

4.1. MIMO Performance Parameters

The radiation gain pattern of each element was obtained by exciting the element and terminating the other elements with $50\,\Omega$ load, and it is observed that the realized gain is -12 dB as shown in Fig. 4(a). The gain for MIMO antenna is -8.9 dB when both the antennas are excited as observed in Fig. 4(b).

The correlation coefficient ρ is a measure that describes how the communication channels are isolated or correlated with each other. High isolation and low correlation coefficients are required for a MIMO antenna system to provide good diversity performance [38]. The square of the correlation coefficient is the Envelope Correlation Coefficient (ECC). The correlation coefficient can be computed by using S parameters and radiation efficiency [38]. Plot of frequency Vs. ECC is shown in Fig. 5, and it is observed that it is approximately zero which is within the acceptable limits of below 0.3 for 4G standards.

Total Active Reflection Coefficient (TARC) is defined as the square root of the ratio of the sum of the power available at all the ports minus the radiated power to the total available power [37]. It is a real number between 0 and 1 [38]. When its value is zero, this means that all the available power is radiated. The proposed antenna has a TARC value of 0.1472 which is within 0 to 1 as shown in Fig. 6.

Channel capacity is the tightest upper bound on the rate of information that can be consistently transmitted over a communications channel [38].

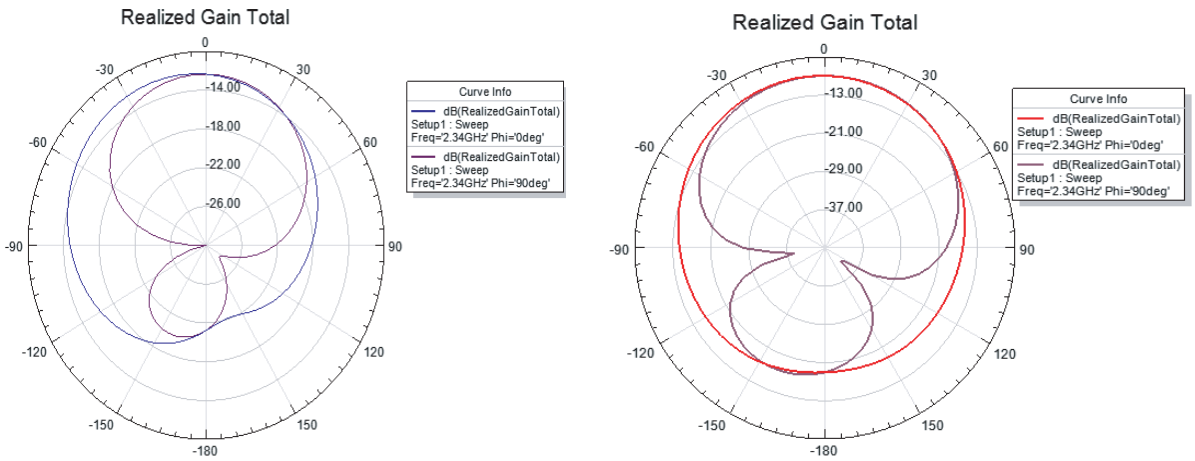

Figure 4. (a) Simulated 2-D radiation pattern for single antenna. (b) Simulated 2-D radiation pattern for MIMO antenna.

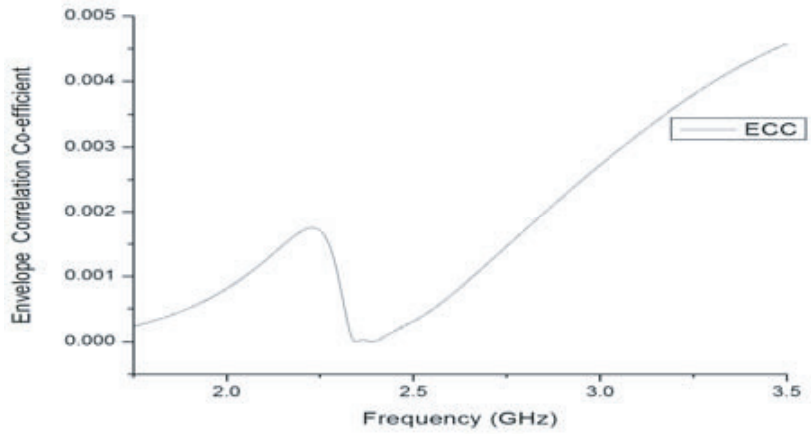

Figure 5. Simulated envelope correlation coefficient.

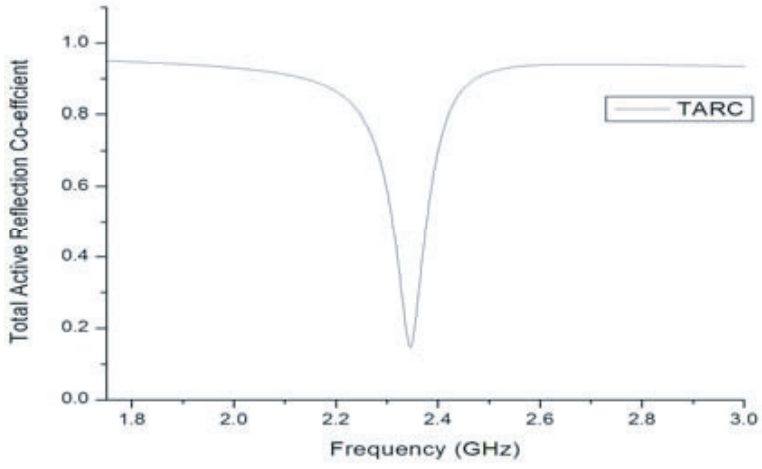

Figure 6. Simulated total active reflection coefficient.

The channel capacity loss is given by

$$C_{loss} = -\log_2 \det(\psi^R) \tag{5}$$

$$\text{where } \psi^R = \begin{bmatrix} \rho_{11} & \rho_{12} \\ \rho_{21} & \rho_{22} \end{bmatrix}, \tag{6}$$

$$\rho_{ii} = 1 - (|S_{ii}|^2 + |S_{ij}|^2) \tag{7}$$

$$\text{and } \rho_{ij} = -(S_{ii}^* S_{ij} + S_{ji}^* S_{ij}), \quad \text{for } i, j = 1 \text{ or } 2 \tag{8}$$

It can be observed from Fig. 7 that the capacity loss is -21.35 b/s/Hz which is computed using Equations (5)–(8,) and it is well below the threshold value 0.4 b/s/Hz [38].

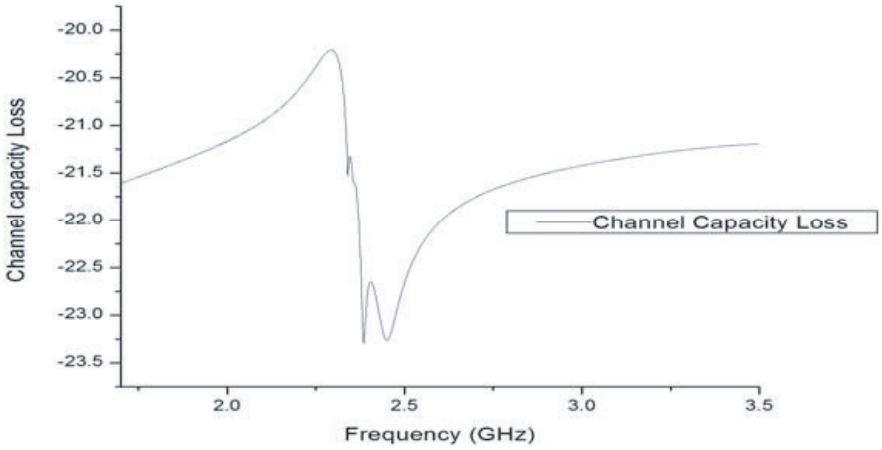

Figure 7. Simulated capacity loss.

5. CONCLUSION

A 2×1 MIMO circular patch antenna is designed and investigated. Using Nicolson Ross Weir technique, permittivity and permeability are calculated, which are negative, clearly indicating that the antenna with CSRR acts as a bandpass filter at the resonant frequency of 2.34 GHz providing miniaturization. Antenna miniaturization of 55.17% was achieved by etching CSRR in the ground plane underneath the patch. The ECC computed using the scattering parameters is 0.000015 for the proposed antenna with TARC as 0.1472 which is within the acceptable limits of 0 to 1. Similarly, the capacity loss remains -21.35 b/s/Hz throughout the LTE band. The total gain is also improved compared to a single patch antenna. The proposed antenna provides a good isolation of -33.5 dB. The antenna performance is suitable for LTE band 40 operation.

ACKNOWLEDGMENT

Authors would like to thank Dr. Yogesh Kumar Choukiker, Associate Professor, VIT University, Vellore, for his valuable time and suggestions throughout the work.

REFERENCES

1. Garg, V. K., *Wireless Communications and Networking*, Elsevier-Morgan Kaufmann, Waltham, MA, 2007.
2. Larmo, A., et al., "The LTE link-layer design," *IEEE Commun. Mag.*, Vol. 47, No. 4, 52–59, Apr. 2009.

3. Zhang, Y. and B. Niu, "Compact Ultrawideband (UWB) slot antenna with wideband and high isolation for MIMO applications," *Progress In Electromagnetics Research C*, Vol. 54, 9–16, 2014.
4. Schaubert, D. and K. Yngvesson, "Experimental study of a microstrip array on high permittivity substrate," *IEEE Transactions on Antennas and Propagation*, Vol. 34, No. 1, 92–97, 1986.
5. Herscovici, N., M. F. Osorio, and C. Peixeiro, "Miniaturization of rectangular microstrip patches using genetic algorithms," *IEEE Antennas and Wireless Propagation Letters*, Vol. 1, No. 1, 94–97, 2002.
6. Bokhari, S. A., et al., "A small microstrip patch antenna with a convenient tuning option," *IEEE Transactions on Antennas and Propagation*, Vol. 44, No. 11, 1521–1528, 1996.
7. Latif, S. I., L. Shafai, and C. Shafai, "An engineered conductor for gain and efficiency improvement of miniaturized microstrip antennas," *IEEE Antennas and Propagation Magazine*, Vol. 55, No. 2, 77–90, 2013.
8. Chow, Y. L., K. L. Wan, and T. K. Sarkar, "Patch antenna miniaturizing with a shorting pin near the feed probe-its physical mechanism and the design on Smith Chart," *2001 Asia-Pacific Microwave Conference, APMC 2001*, Vol. 3, IEEE, 2001.
9. Kuo, J.-S. and K.-L. Wong, "A compact microstrip antenna with meandering slots in the ground plane," *Microwave and Optical Technology Letters*, Vol. 29, No. 2, 95–97, 2001.
10. Huang, J., "The finite ground plane effect on the microstrip antenna radiation patterns," *IEEE Transactions on Antennas and Propagation*, Vol. 31, No. 4, 649–653, 1983.
11. Liu, J., W.-Y. Yin, and S. He, "A new defected ground structure and its application for miniaturized switchable antenna," *Progress In Electromagnetics Research*, Vol. 107, 115–128, 2010.
12. Khan, M. U., M. S. Sharawi and R. Mittra, "Microstrip patch antenna miniaturisation techniques: A review," *IET Microwaves, Antennas & Propagation*, Vol. 9, No. 9, 913–922, Jun. 2015.
13. Dong, Y., H. Toyao, and T. Itoh, "Design and characterization of miniaturized patch antenna loaded with complementary split ring resonators," *IEEE Transactions on Antennas and Propagation*, Vol. 60, No. 2, 772–785, Feb. 2012.
14. Ouedraogo, R. O., E. J. Rothwell, A. R. Diaz, K. Fuchi, and A. Temme, "Miniaturization of patch antennas using a metamaterial-inspired technique," *IEEE Transactions on Antennas and Propagation*, Vol. 60, No. 5, 2175–2182, May 2012.
15. Khan, M. U. and M. S. Sharawi, "A compact 8-element MIMO antenna system for 802.11ac WLAN applications," *International Workshop on Antenna Technology, (IWAT)*, 91–94, 2013.
16. Asieh, H., J. Nourinia/ and C. Ghobadi, "Mutual coupling reduction between very closely spaced patch antennas using low-profile Folded Split-Ring Resonators (FSRRs)," *IEEE Antennas and Wireless Propagation Letters*, Vol. 10, 862–865, IEEE, 2011.
17. Saraswat, R. K. and M. Kumar, "Miniaturized slotted ground UWB antenna loaded with metamaterial for WLAN and WiMAX applications," *Progress In Electromagnetics Research B*, Vol. 65, 65–80, 2016.
18. Liu, L., S. W. Cheung, and T. Yuk, "Compact MIMO antenna for portable UWB applications with band-notched characteristic," *IEEE Transactions on Antennas and Propagation*, Vol. 63, No. 5, 1917–1924, 2015.
19. Xia, R., S. Qu, Q. Jiang, P. Li, and Z. Nie, "An efficient decoupling feeding network for two-element microstrip antenna array," *IEEE Transactions on Antennas and Wireless Propagation Letters*, Vol. 14, 871–874, 2015.
20. Lin, K.-C., C.-H. Wu, C.-H. Lai, and T.-G. Ma, "Novel dual-band decoupling network for two-element closely spaced array using synthesized microstrip lines," *IEEE Transactions on Antennas and Propagation*, Vol. 60, No. 11, 5118–5128, 2012.
21. Chen, W.-J. and H.-H. Lin, "LTE700/WWAN MIMO antenna system integrated with decoupling structure for isolation improvement," *Antennas and Propagation Society International Symposium (APSURSI)*, 689–690, IEEE, 2014.
22. Wang, H., D. G. Fang, and X. L. Wang, "Mutual coupling reduction between two microstrip patch antennas by using the parasitic elements," *Asia-Pacific Microwave Conference, APMC 2008*, 1–4,

IEEE, 2008.

23. Margaret, D. H., M. R. Subasree, S. Susithra, S. S. Keerthika, and B. Manimegalai, "Mutual coupling reduction in MIMO antenna system using EBG structures," *International Conference on Signal Processing and Communications (SPCOM)*, 1–5, IEEE, 2012.
24. Islam, M. T. and M. S. Alam, "Compact EBG structure for alleviating mutual coupling between patch antenna array elements," *Progress In Electromagnetics Research*, Vol. 137, 425–438, 2013.
25. Yu, Y., et al., "Dual-frequency two-element antenna array with suppressed mutual coupling," *International Journal of Antennas and Propagation*, 1–6, 2014.
26. Wu, Y.-T. and Q.-X. Chu, "Dual-band multiple input multiple output antenna with slitted ground," *Microwaves, Antennas & Propagation*, IET 8.13, 1007–1013, 2014.
27. Su, S.-W., C.-T. Lee, and F.-S. Chang, "Printed MIMO-antenna system using neutralization-line technique for wireless USB-dongle applications," *IEEE Transactions on Antennas and Propagation*, Vol. 60, No. 2, 456–463, 2012.
28. Zhang, S. and G. Pedersen, "Mutual coupling reduction for UWB MIMO antennas with a wideband neutralization line," *IEEE Antennas and Wireless Propagation Letters*, Vol. 15, 166–169, 2016.
29. Ren, Y.-H., et al., "A wideband dual-polarized printed antenna based on complementary split-ring resonators," *IEEE Antennas and Wireless Propagation Letters*, Vol. 14, 410–413, 2015.
30. Baena, J. D., J. Bonache, F. Martin, R. Marques, F. Falcone, T. Lopetegi, M. A. G. Laso, J. Garcia, I. Gil, and M. Sorolla, "Equivalent-circuit models for split-ring resonators and complementary split-ring resonators coupled to planar transmission lines," *IEEE Transactions on Microwave Theory and Techniques*, Vol. 53, No. 4, 1451–1461, Apr. 2005.
31. Wahid, A., M. Sreenivasan, and P. H. Rao, "CSRR loaded microstrip array antenna with low sidelobe level," *IEEE Antennas and Wireless Propagation Letters*, Vol. 14, 1169–1171, 2015.
32. Cheng, X., D. E. Senior, C. Kim, and Y. Yoon, "A compact omnidirectional self-packaged patch antenna with complementary split-ring resonator loading for wireless endoscope applications," *IEEE Antennas and Wireless Propagation Letters*, Vol. 10, 1532–1535, 2011.
33. Ziolkowski, R. W., "Design, fabrication and testing of double negative metamaterials," *IEEE Transactions on Antennas and Propagation*, Vol. 51, No. 7, 1516–1529, Jul. 2003.
34. Rothwell, E. J., et al., "Analysis of the Nicolson-Ross-Weir Method for characterizing the electromagnetic properties of engineered materials," *Progress In Electromagnetics Research*, Vol. 157, 31–47, 2016.
35. Wirgin, A., "Retrieval of the frequency-dependent effective permeability and permittivity of the inhomogeneous material in a layer," *Progress In Electromagnetics Research B*, Vol. 70, 131–147, 2016.
36. Luo, C.-M., J.-S. Hong, and L.-L. Zhong, "Isolation enhancement of a very compact UWB-MIMO slot antenna with two defected ground structures," *IEEE Transactions on Antennas and Propagation*, Vol. 14, No. 2, 1766–1769, Apr. 2015.
37. Sharawi, M. S., M. U. Khan, A. B. Numan, and D. N. Aloi, "A CSRR loaded MIMO antenna system for ISM band operation," *IEEE Transactions on Antennas and Propagation*, Vol. 61, No. 8, 4265–4274, Aug. 2013.
38. Choukiker, Y. K., S. K. Sharma, and S. K. Behera, "Hybrid fractal shape planar monopole antenna covering multiband wireless communications with MIMO implementation for handheld mobile devices," *IEEE Transactions on Antennas and Propagation*, Vol. 62, No. 3, 1483–1488, Mar. 2014.